Aerosol Spray Pyrolysis Synthesis of Magnetic Manganese Ferrite Particles

Qiang Li and C. M. Sorensen*
Department of Physics, Kansas State University, Manhattan, KS 66506

K. J. Klabunde
Department of Chemistry, Kansas State University, Manhattan, KS 66506

G. C. Hadjipanayis
Department of Physics & Astronomy, University of Delaware, Newark, DE 19716

We describe the aerosol spray pyrolysis synthesis and subsequent properties of manganese ferrite ($MnFe_2O_4$) submicrometer particles. Various combinations of the chlorides and nitrates of manganese and iron dissolved in water were used as precursors. Typical aerosol reactor residence times were 0.5–1.5s. With insufficient reactor temperature, e.g., 650°C, porous, hollow particles with a mixture of the ferrite and the individual metal oxides were obtained. These intermediate phases and morphologies were precursor dependent. In particular, nitrate ion caused oxidization of the manganese to the trivalent state, which is unsuitable for ferrite formation and caused what we termed a chemical segregation of the phases. Postaerosol baking showed how these particles evolved to dense, single-phase, agglomerated ferrite particles. If instead the aerosol reactor was at a sufficiently high temperature, > 900°C, dense, single-phase, unagglomerated particles were formed in one aerosol step. The particles had nearly bulklike magnetic properties except for effects that could be ascribed to the submicrometer size of the particles and the rapid thermal quenching as the particles left the reactor.

INTRODUCTION

Gas-phase aerosol synthesis techniques offer an attractive route for the production of particulates as precursors for ceramic materials. One such method, aerosol spray pyrolysis, has seen considerable effort in the last decade (Roy et al., 1977; Ruthner, 1983; Sproson et al., 1986; Kodas, 1989). This method, simple in concept, involves dissolution of precursor salts, nebulizing the solution, drying and reacting the droplets in a heated reactor, and then collection of the particles. The technique has a number of positive attributes. Relatively pure particles in the submicrometer range can be produced. A wide range of chemical compositions can be created including complex, multicomponent systems. Each droplet acts as a microreactor in which the constituents are mixed on the atomic level hence particle homogeneity is expected. The method has the potential for continuous creation of particles in one step.

Two major disadvantages of aerosol spray pyrolysis involve particle morphology and phase homogeneity. Very often hollow or porous particles are created. Such nondense particulates are not suitable for further ceramic processing. This problem has been a major issue of late (Zhang et al., 1990; Ortega et al., 1991;

* To whom correspondence should be addressed.

Aerosol Science and Technology 19:453–467 (1993)

0278-6826/93/$6.00

Ortega and Kodas, 1992). It is due to surface precipitation in the droplet during the drying and/or reactor step (Charlesworth and Marshall, 1960). Slow drying or use of high solubility salts (so the relative saturation can be low) (Zhang et al., 1990) or high-temperature aerosol phase densification (Orgeta et al., 1991) have been advocated to alleviate this problem. Porosity can occur regardless of whether the particles are uniform or hollow. This may result during heating of the dried salts as water of hydration and/or volatile anions leave the particle. Another common problem involves phase inhomogeneity or phase segregation hence the appearance of unwanted phases in the particles, despite the initial atomic level mixing of the precursor solution. This is an important problem since it degrades one of the major attributes of aerosol spray pyrolysis, the ability to create complex, multicomponent systems. Phase segregation can occur during the drying step owing to a number of causes including differential precipitation of the components due to solubility differences, lack of isomorphic crystallization, differential reactions during drying, and a process that we will develop in this article, chemical segregation.

To date the literature describing aerosol spray pyrolysis has been largely, and properly, concerned with the problems outlined in the preceding paragraphs, and less attention has been given to the end-use physical and chemical properties of the particles. As the maturity of this method develops, however, it is appropriate that concern grows regarding particle end-use properties. This has already occurred to an extent for particles of the new high-T_c superconductors (Chadda et al., 1991; Zhang et al., 1991) and for magnetic particles (Tang et al., 1989 a,b; Biswas et al., 1992; Xu et al., 1992). The motive behind our work has been to produce particles of magnetic materials and see what effects, if any, aerosol spray pyrolysis synthesis has on their magnetic properties. Furthermore, for practical application it is important to make these particles dense and phase pure.

In this article we describe the aerosol spray pyrolysis synthesis of manganese ferrite ($MnO \cdot Fe_2O_3$ or $MnFe_2O_4$), which is a cubic ferrite, hence soft magnetic material (Cullity, 1972). We have used precursors of both the chlorides and nitrates of iron and manganese. The main result is that unagglomerated, dense, chemically and magnetically single-phase particles of manganese ferrite can be produced in a one-step aerosol processes. The key to achieving these desirable properties is sufficient heating in the aerosol reactor. Otherwise hollow and/or porous particles result that are a mixture of the ferrite and various other oxides of the precursor metals. The phase inhomogeneity is due to partial oxidization of the divalent manganese ion by nitrate present in some of the precursors. We find that temperature is more important than time to achieve the desired ferrite phase. The magnetic properties were essentially those of the bulk ferrite although both the small size and the aerosol preparation process had some effect on the saturation magnetization, coercivity, and Curie temperature.

EXPERIMENTAL METHODS

Precursor solutions were made up in distilled, deionized water from various combinations of $FeCl_3 \cdot 6H_2O$, $Fe(NO_3)_3 \cdot 6H_2O$, $MnCl_2 \cdot 4H_2O$, and $Mn(NO_3)_2 \cdot 4H_2O$. Some physical properties of these salts, e.g., solubility, are given in Table 1. Solutions with mixtures of the metal cations always had an atomic ratio of $Mn/Fe = 1/2$. The total metal ion concentration was $[Mn^{+2}] + [Fe^{+3}] = 0.0875$ mol/L. Some solutions were made up at 1/2 and 1/10 this value.

TABLE 1. Physical Properties of the Precursor Salts (Weast, 1977)

Salt	Water solubility (g/100 μL) Cold	Hot (100°C)	T_{melt} (°C)	T_{boil} (°C)
$FeCl_3 \cdot 6H_2O$	92 (20°C)	∞	37	280
$Fe(NO_3)_3 \cdot 6H_2O$	150 (0°C)	∞	35	decomposes
$MnCl_2 \cdot 4H_2O$	151 (8°C)	656	58	$-4\ H_2O$, 198°C 1190
$Mn(NO_3)_2 \cdot 4H_2O$	426 (0°C)	∞	26	129

These solutions were processed through our spray pyrolysis apparatus which consisted of an atomizer, drier, tube furnace reactor, and collection filter. Nebulization of the solutions was accomplished with a constant output atomizer (Model 3075, TSI Inc., St. Paul, MN), which yields droplets with a mean diameter somewhat < 1 μm. The carrier gas was nitrogen at an input pressure of 35 psig producing a gas flow of 2.6 L/min and a solution nebulization rate of 5 mL/hour. The aerosol then typically passed through a diffusion drier which consisted of a tubular screen 50 cm long, 2 cm in diameter, and surrounded by the dessicant, $CaSO_4$. The aerosol then passed into a tube furnace reactor. The quartz reactor tube had a 2.0 cm inside diameter. Up to three sections of furnace, each 30 cm long could be used to heat this quartz tube. Later, when we specify our reactor temperature, we will quote the temperatures of these furnaces as they are encountered serially by the aerosol, if they are above room temperature. Aerosol residence times in the hot portion of the reactor are a function of flow rate, tube diameter, and temperature. For 900°C reactors the residence time is $t_R \sim 0.5$ s per 30-cm section.

After the reactor, the aerosol particles were collected on a fritted glass filter. The powders were either used as-prepared or subjected to further baking under nitrogen or argon in alumina coated tungsten boats in the tube furnace. Characterization was achieved with x-ray diffraction (XRD, Cu K α), transmission electron microscopy (TEM), and BET surface analysis which yields the specific surface area S(m^2/g). The magnetic properties were measured with a SQUID Magnetometer (Quantum Design Model MPMS 5) equipped with an oven to allow for temperatures up to 800K.

The XRD data were used to make a semiquantitative analysis of the phases. To find the fraction of ferrite present in a sample, we measured the intensity of the strongest line of the ferrite I_F and the strongest lines of any other phases I_i present (all oxides). We then define a measure of the percentage of ferrite present by $F\% = 100 I_F/(I_F + \Sigma I_i)$ (Klug and Alexander, 1954). This measure is quantitative only when $F\% \to 100\%$, but it is very useful as a qualitative descriptor of phase evolution. The width of the XRD lines gave crystallite effective diameters through the Scherrer formula (Klug and Alexander, 1954). The BET analysis can be used to calculate an effective particle diameter from the specific surface area using $d = 6/\rho S$, where ρ is the particle density which we took as 5.0 g/cm^3, the density of bulk $MnFe_2O_4$.

General results for all the as-prepared samples are given in Table 2. In what follows we describe in detail the properties of these samples.

TABLE 2. As-Prepared Samples

Precursors	Reactor temp. (°C)	XRD	BET (m^2/g)	TEM	σ_s (emu/g) (300 K)	H_c (Oe) (300 K)	T_c (K)
$MnCl_2 + FeCl_3$	650	Ferrite $d \sim 10$ nm (Amorphous oxides)	51 $d \sim 24$ nm	Core-shell porous $d \sim 150$ nm	Paramagnetic		
$Mn(NO_3)_2 + FeCl_3$	650	Ferrite, Fe_2O_3 Mn_2O_3, Mn_3O_4	—	Hollow, porous	Paramagnetic		
$Mn(NO_3)_2 + FeCl_3$	1050	Ferrite $d \sim 27$ nm	—	Hollow	73	17	593
$Mn(NO_3)_2 + FeCl_3$	250 + 1050	Ferrite $d \sim 27$ nm	9.4 $d \sim 130$ nm	Some hollow $d \sim 110$ nm	80	—	596
$Mn(NO_3)_2 + FeCl_3$ (1/10 concn)	900 + 1050	Ferrite	—	Solid	70	55	593
$MnCl_2 + Fe(NO_3)$	650	Fe_2O_3, Mn_2O_3	—	Some Hollow	Paramagnetic		
$Mn(NO_3)_2 + Fe(NO_3)_3$	250	Amorphous	—	Uniform, porous $d \sim 150$ nm	Paramagnetic		
$Mn(NO_3)_2 + Fe(NO_3)_3$	650	Fe_2O_3, Mn_2O_3	70 $d \sim 17$ nm	Nonhollow porous spheres $d \sim 150$ nm	Paramagnetic		
$Mn(NO_3)_2 + Fe(NO_3)_3$	1050	60% Ferrite Fe_2O_3, Mn_2O_3	—	Solid, nonuniform	27	16	490
$Mn(NO_3)_2 + Fe(NO_3)_3$	250 + 1050	95% Ferrite	—	Solid $d \sim 80$ nm	64	20	—
$Mn(NO_3)_2 + Fe(NO_3)_3$	900 + 1050	—	—	Solid, polygonal $d \sim 80$ nm	78	36	587
$Mn(NO_3)_2 + Fe(NO_3)_3$	900 + 1050 + 900	Ferrite	—	Solid polygonal $d \sim 80$ nm	82	50	584
$Mn(NO_3)_2 + Fe(NO_3)_3$	900 + 1250 900	Ferrite	—	Solid polygonal $d \sim 80$ nm	80	30	—
$Mn(NO_3)_2 + Fe(NO_3)_3$ 1/2 concn	900 + 1050	—	—	Solid polygonal $d \sim 60$ nm	76	50	594
$Mn(NO_3)_2 + Fe(NO_3)_3$ 1/10 concn	900 + 1050	—	—	Solid polygonal $d \sim 40$ nm	71	56	~585

RESULTS

As-Prepared, 650°C Reactor Products: Phases

As outlined in Table 2, the 650°C aerosol reactor products had incomplete morphology and phase compared to the desired dense, single-phase ferrite particles. Table 3 gives phase information as determined by XRD. We note that XRD of the Cl/Cl product showed the individual metal oxides Fe_2O_3 and Mn_2O_3 only after further, postaerosol heat treatment at 600°C for 2 h. Further heat treatment for all samples caused the ferrite phase to increase at the expense of the individual oxide phases. These facts indicate that the individual oxides were present in the as-prepared Cl/Cl product in the amorphous form hence not detected with XRD.

Table 3 demonstrates an anticorrelation between the ferrite phase in the as-

TABLE 3. Compositions of As-Prepared, 650°C Reactor Products

Precursors	Precursor soln. NO_3^- concn (mol/L)	Composition
$Fe(NO_3)_3 + Mn(NO_3)_2$	0.23	Fe_2O_3, Mn_2O_3
$Fe(NO_3)_3 + MnCl_2$	0.175	Fe_2O_3, Mn_2O_3
$FeCl_3 + Mn(NO_3)_2$	0.058	Fe_2O_3, Mn_2O_3, $MnFe_2O_4$, Mn_3O_4
$FeCl_3 + MnCl_2$	0	$MnFe_2O_4$, Fe_2O_3, Mn_2O_3
$FeCl_3$	0	Fe_2O_3
$MnCl_2$	0	Mn_3O_4, MnO

prepared particles and the nitrate ion concentration, $[NO_3^-]$, in the precursor solution. Furthermore, there is a direct correlation between $[NO_3^-]$ and Mn^{3+} found in the particles in the form of the oxides Mn_2O_3 and Mn_3O_4. Thus it appears that the nitrate ion oxidizes the Mn^{2+} of the precursor

$$Mn^{2+} \rightarrow Mn^{3+} + e^- . \quad (1)$$

Since Mn^{2+} is necessary for the formation of the ferrite, anticorrelation between $[NO_3^-]$ and ferrite formation occurs.

It is valuable to compare our results to those of Gadalla and co-workers (Clearfield et al., 1989; Gadalla and Yu, 1990), who used aerosol spray pyrolysis to create nickel ferrite, $NiFe_2O_4$, from $Ni(NO_3)_2$ and $Fe(NO_3)_3$ precursors. No phase segregation occurred in their system; only $NiFe_2O_4$ was formed. The difference in phase segregation behavior between these two very similar ferrites is most likely caused by the fact that the nickle ion, Ni^{2+}, cannot be oxidized to the trivalent state. Hence, in contrast to the $MnFe_2O_4$ system, there is no tendency to form the trivalent state which is wrong for ferrite formation and would lead to other oxides. This trivalency can occur in the manganese system, more so with increasing $[NO_3^-]$. Also, given the similarities in precursor salt concentrations, ionic radii, and reactivity with water for the precursor salts of both ferrites, we assert that the tendency for Mn^{2+} to be oxidized by the $[NO_3^-]$ is the only reason for phase segregation in our system. We shall call this process "chemical segregation."

As-Prepared, 650°C Reactor Products: Morphology

TEM micrographs of the $MnCl_2/FeCl_3$ and $Mn(NO_3)_2/Fe(NO_3)_3$ precursors, as-prepared particles collected after the 650°C furnace are given in Figure 1, a and b, respectively. The Cl/Cl particles are grainy and many are spherical shells partially filled with smaller spherical cores. The NO_3/NO_3 particles are uniformly grainy and do not have this core-shell structure. Both systems have an average overall particle size of ~150 nm as observed in the TEM. However, sizes determined from BET surface area measurements are significantly smaller: Cl/Cl, $S = 51$ m^2/g to imply an effective diameter of 24 nm; and NO_3/NO_3, $S = 70$ m^2/g to imply an effective diameter of 17 nm. Furthermore, the crystallite size determined from the XRD linewidth and the Scherrer formula is 10 nm for the Cl/Cl system. All these results indicate that the particles are nondense, porous and multicrystalline with the Cl/Cl particles somewhat more so than the NO_3/NO_3 particles.

We also created NO_3/NO_3 precursor particles with a 250°C furnace. This system was XRD amorphous. The TEM micrograph of this product in Figure 2 shows homogeneous spherical particles, again $d_{TEM} \sim 150$ nm. Comparison to Figure 1b

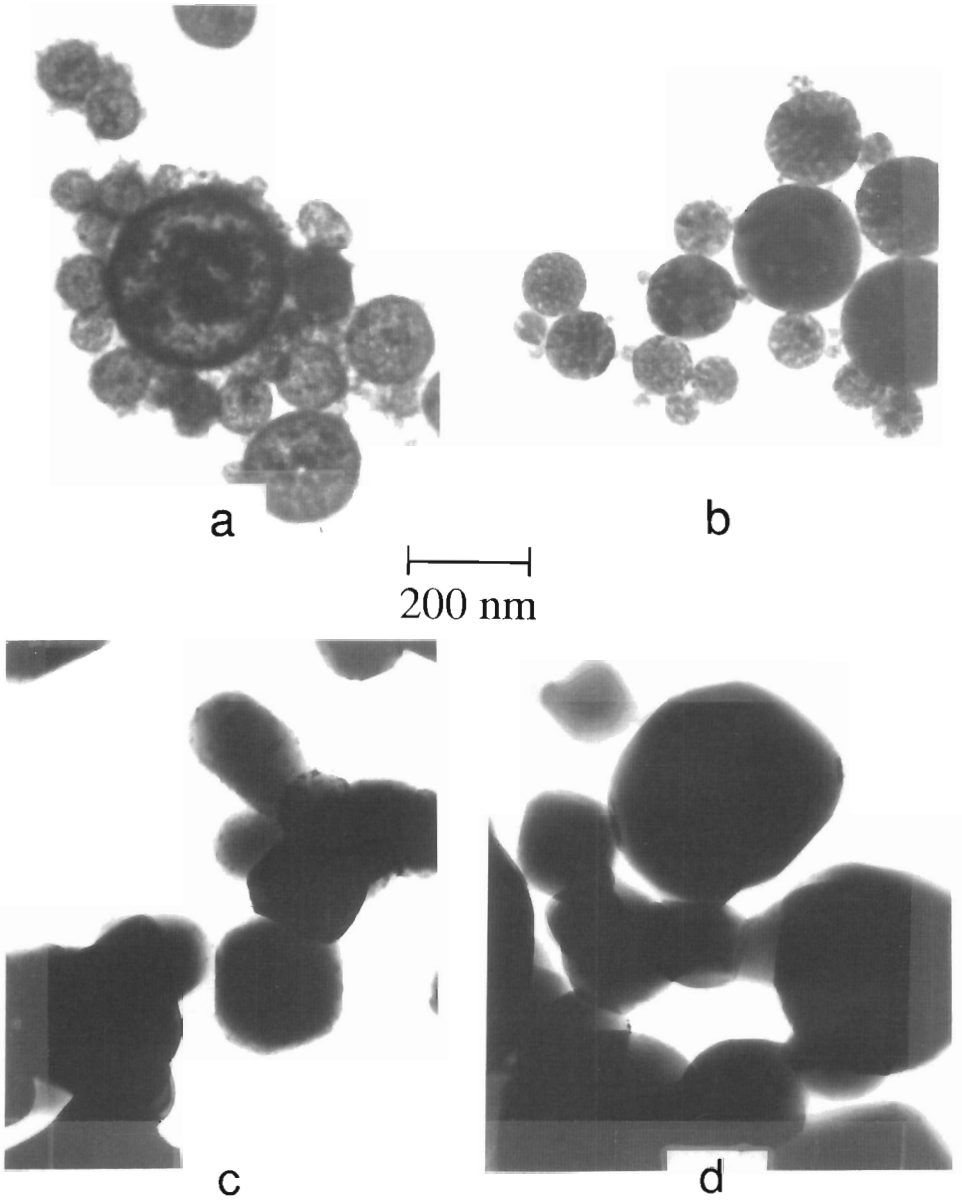

FIGURE 1. TEM micrographs of 650°C aerosol reactor particles: (a) Cl/Cl precursor as-prepared; (b) NO_3/NO_3 precursor, as-prepared; (c) Cl/Cl precursor as-prepared product baked at 900°C for 14 h; (d) NO_3/NO_3 precursor as-prepared product baked at 900°C for 14 h.

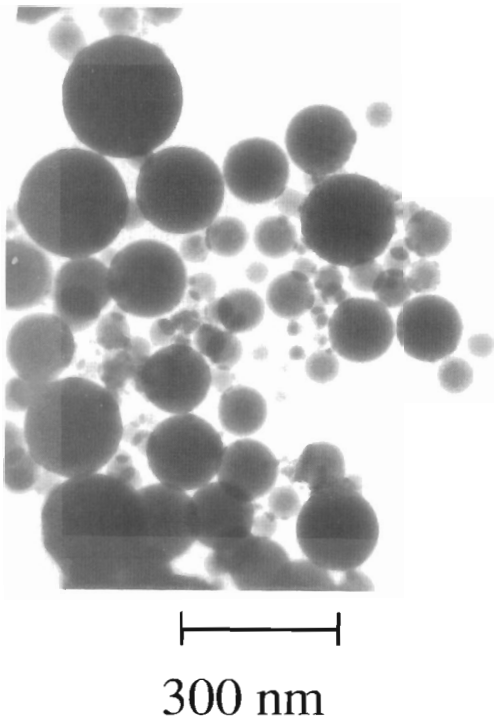

FIGURE 2. TEM micrograph of as-prepared NO_3/NO_3 precursor, 250°C aerosol reactor particles.

shows a much finer grain structure for the 250°C product. This may be due to the milder condition of pyrolysis.

We conclude by noting that all these products were paramagnetic.

Postaerosol Baking Study: Phases

The 650°C aerosol reactor products described above were subjected to postaerosol baking heat treatments under an inert gas to watch the evolution of phase, morphology, and magnetic properties. The inert gas was either nitrogen or argon, and no difference with these gases was observed.

Phase evolution as a function of time and baking temperatures is illustrated in Figures 3 and 4, respectively. The relative concentration of the ferrite could not be determined in the as-prepared particles of the Cl/Cl system because no individual metal oxide lines where present in the XRD spectrum. As described above, this presumably is due to the amorphous nature of these oxides in these particles. Heat treatment at 600°C for 2 h yielded XRD spectra with sharp lines of, presumably, all phases present, so a concentration measurement could be made. One

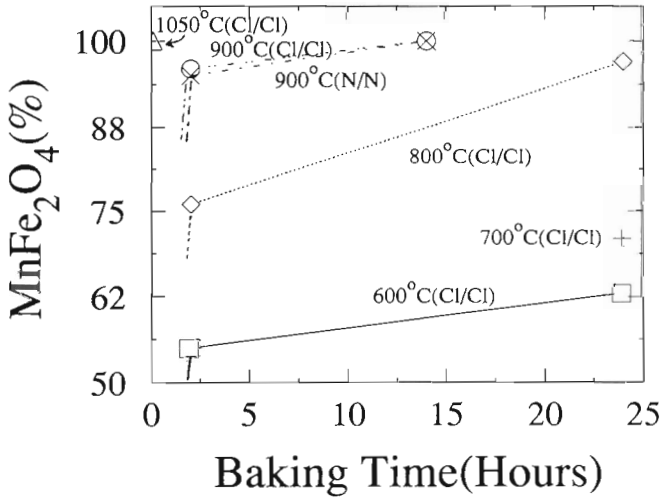

FIGURE 3. Percentage fraction of the $MnFe_2O_4$ phase as a function of baking time. Label for each curve gives the baking temperature and, in parentheses, the precursor.

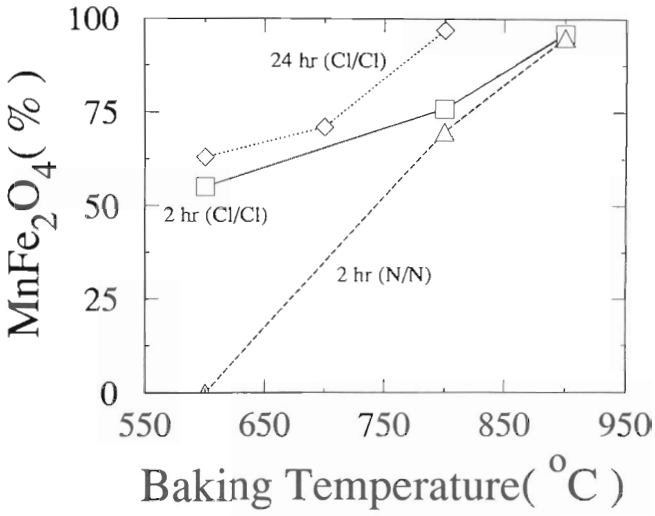

FIGURE 4. Percentage fraction of the $MnFe_2O_4$ phase as a function of baking temperature. Label for each curve gives the baking time and, in parentheses, the precursor.

may infer that the as-prepared samples have a ferrite concentration less than or equal to the composition found for the 600°C, 2-h heat treatment, which was 55% ferrite. This is accounted for in Figure 3 which indicates a large jump in ferrite fraction after 2 h of baking. The ferrite composition then levels off with longer time to a value that is strongly temperature dependent. In general, we find, as shown in Figures 3 and 4, that both higher temperature and longer duration heat treatment shifts the equilibrium in Eq. 2 to the right.

$$Mn_2O_3 + 2Fe_2O_3 \rightleftarrows 2MnFe_2O_4 + 1/2\ O_2. \quad (2)$$

Figures 3 and 4 also allow us to compare the phase evolution of the two precursor systems. Figure 4 shows a 600°C heat treatment for 2 h for the NO_3/NO_3 system yielded no ferrite, whereas the Cl/Cl system had 55% ferrite. At higher temperatures the NO_3/NO_3 system begins to catch up with the Cl/Cl system, the 900°C isotherms in Figure 3 being identical to within experimental error. This confluence is illustrated in Figure 4 where we plot ferrite fraction versus temperature for various times. The NO_3/NO_3 system starts way behind the Cl/Cl, due to chemical segregation, but for $T \gtrsim 900$°C both systems evolve to the 100 % ferrite situation.

Postaerosol Baking Study: Morphology

Morphologic evolution obvious to the naked eye was significant shrinkage of the powders and their apparent sintering together to form a hard cake when baked at temperatures of 900°C or greater. Also a color change from dark brown to black was seen for $T \gtrsim 900$°C Figure 1, c and d shows TEM micrographs of the Cl/Cl and NO_3/NO_3 systems, respectively, both after 900°C, 14 h baking. Both show uniform, dense, spherical-to-polygonal particles indicating full densification has occurred. Both indicate that coalescence of smaller particles into larger ones seems to have occurred when compared to the unbaked samples in Figure 1, a and b, and the mean particle size inferred from TEM is ~ 250 nm, larger than before baking. Furthermore, significant necking between particles is visible indicating particle sintering and agglomeration. BET measurements on the Cl/Cl sample went from

$S = 51$ to ≤ 2 m^2/g after 900°C baking for 14 h. The inferred size from $S = 2$ m^2/g is 150 nm, which is comparable to the size determined from the TEM, implying that the particles are no longer porous. (However, we note this small S value is at the lower limit of measurability with our apparatus.)

Postaerosol Baking Study: Magnetic Properties

The magnetic properties of these two systems after baking are given in Table 4. Saturation magnetizations were essentially those of the bulk ferrite which is $\sigma_s \simeq 80$ emu/g at 300K and coercivities were typical of soft, cubic ferrite materials like $MnFe_2O_4$ (Cullity, 1972). Note how the short, 5-min, 1050°C baking was as effective as the long, 14-h, 900°C baking for obtaining bulk magnetic properties. Low field σ vs. T curves for two of these samples are shown in Figure 5. These curves are typical for single component magnetic systems, hence the particles are magnetically uniform. The value of σ_s and, in particular, the Curie temperature, T_c, can vary somewhat depending on the distribution of the Mn^{2+} ions between the tetrahedral A sites and octahedral B sites of the spinel lattice. The "normal" or equilibrium distribution is ~80% of the manganese in the A sites and 20% in the B sites (Cullity, 1972). This can vary as a function of preparation method and heat treatment and subsequent cooling rates (Yasuoka et al., 1967; Simsa and Brabers, 1975). For this 80/20 distribution $\sigma_s = 80$ emu/g and $T_c = 573$K (Cullity, 1972). Correlation of this ratio to σ_s values are often difficult because a variety of factors including specimen purity and surface effects, however, T_c often correlates well. Both 900°C bakings in Table 4 were cooled slowly, ~5K/min, to room temperature, whereas the 1050°C baking was cooled quickly, ~150K/min, to room temperature. This latter sample has a T_c 35–40K higher than the former ones. The Cl/Cl, 900°C, 14-h sample was reheated to 600°C for 30 min and then quickly cooled to room temperature. Figure 5 shows a significant change in σ vs. T occurred because of this quick cooling and the sample is now quite similar to the other quickly cooled sample. Similar changes in T_c with cooling rate have been observed before for the $MnFe_2O_4$ system.

Aerosol Products: Phase and Morphology

We have seen that dense, phase-pure, submicrometer $MnFe_2O_4$ particles with bulk, single-phase magnetic properties can be created with a two-step process that includes postaerosol baking. However, powder baking caused powder sintering and shrinkage to hard, cakelike products and particle agglomeration through necking. This is not desirable for further ceramic processing. Thus we have, so far, fallen short of our ultimate goal, which is to make a high-quality powder in a single, aerosol step. The baking studies have given valuable lessons, however, because they indicate limits and conditions that we must follow to create, as simply as possible, these single-step powders. The lessons are that the best precursor for phase considerations are Cl/Cl whereas the best precursors for morphology are NO_3/NO_3.

TABLE 4. Magnetic properties of 650°C Aerosol Products after Baking as Specified

Precursor	Heat treatment	σ_s (emu/g) (300K)	H_c(Oe) (300K)	T_c (K)
$FeCl_3/MnCl_2$	900°C, 14 h	76	50	557
$FeCl_3/MnCl_2$	1050°C, 5 min	83	32	598
$Fe(NO_3)_3/Mn(NO_3)_2$	900°C, 14 h	86	0	564

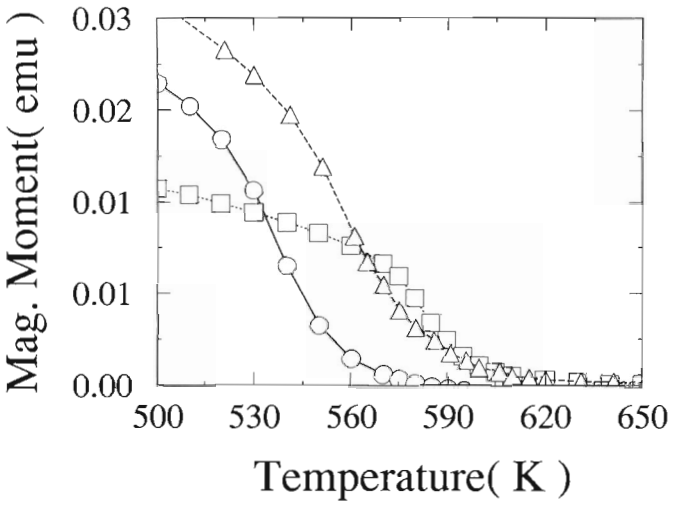

FIGURE 5. Low field ($H = 20$ Oe) magnetic moment versus temperature curves for three Cl/Cl precursor, 650°C aerosol reactor systems after various heat treatments: (□) 1050°C for 5 min, quickly cooled; (○) 900°C for 14 h, slowly cooled; (△) same sample as (○), only reheated to 600°C for 30 min, and quickly cooled.

Temperature is more effective than time in phase evolution, especially temperatures greater than 900°C.

Given these considerations, we chose two precursor systems to study for a single-step aerosol process. Our choice was based on a desire to ensure good morphology for our particles. Thus the NO_3/NO_3 system was used again. As a compromise between the the two 650°C aerosol systems, we also studied, to a lesser extent, a $Mn(NO_3)_2/FeCl_3$ precursor system. These choices are somewhat arbitrary and were made to delimit the number of systems studied. In hindsight we believe the Cl/Cl system would have been equally successful in creating dense, single-phase particles as these two systems. Aerosol particles for both the NO_3/NO_3 and NO_3/Cl systems were subjected to a series of reactor temperatures and the resulting morphology, phase, and magnetic properties were measured.

Comparison of the two systems can be made using Table 2. For a given reactor temperature sequence the NO_3/NO_3 system always has a better morphology but a worse ferrite composition than the NO_3/Cl system. This is in accord with our observations on the postaerosol baked samples of the NO_3/NO_3 and Cl/Cl systems. Dense ferrite particles could be made with the NO_3/Cl system, (Figure 6a), but we chose the NO_3/NO_3 system for further study with greater aerosol heat treatments.

Figure 7 shows XRD spectra for the NO_3/NO_3 system for different aerosol reactor heatings. As reactor temperature and duration increase, an evolution to the pure ferrite with narrow lines is seen. The narrowing of the XRD lines indicates a growth of the crystallites. The lines narrowed to our instrumental linewidth which limits our ability to measure the crystallite size to ≤ 30 nm, hence we cannot determine whether or not the particles are single crystals.

Figure 8 plots the ferrite fraction as a function of reactor heating. Obviously, chemical phase homogeneity can be achieved with sufficient heating. Also plotted in Figure 8 is the saturation magnetization σ_s at 300K versus the reactor heating, which is seen to rise to the bulk value as the ferrite composition becomes 100%.

The particles densified with increasing reactor temperature and duration. Figure 6, b and c, shows TEM micrographs of the

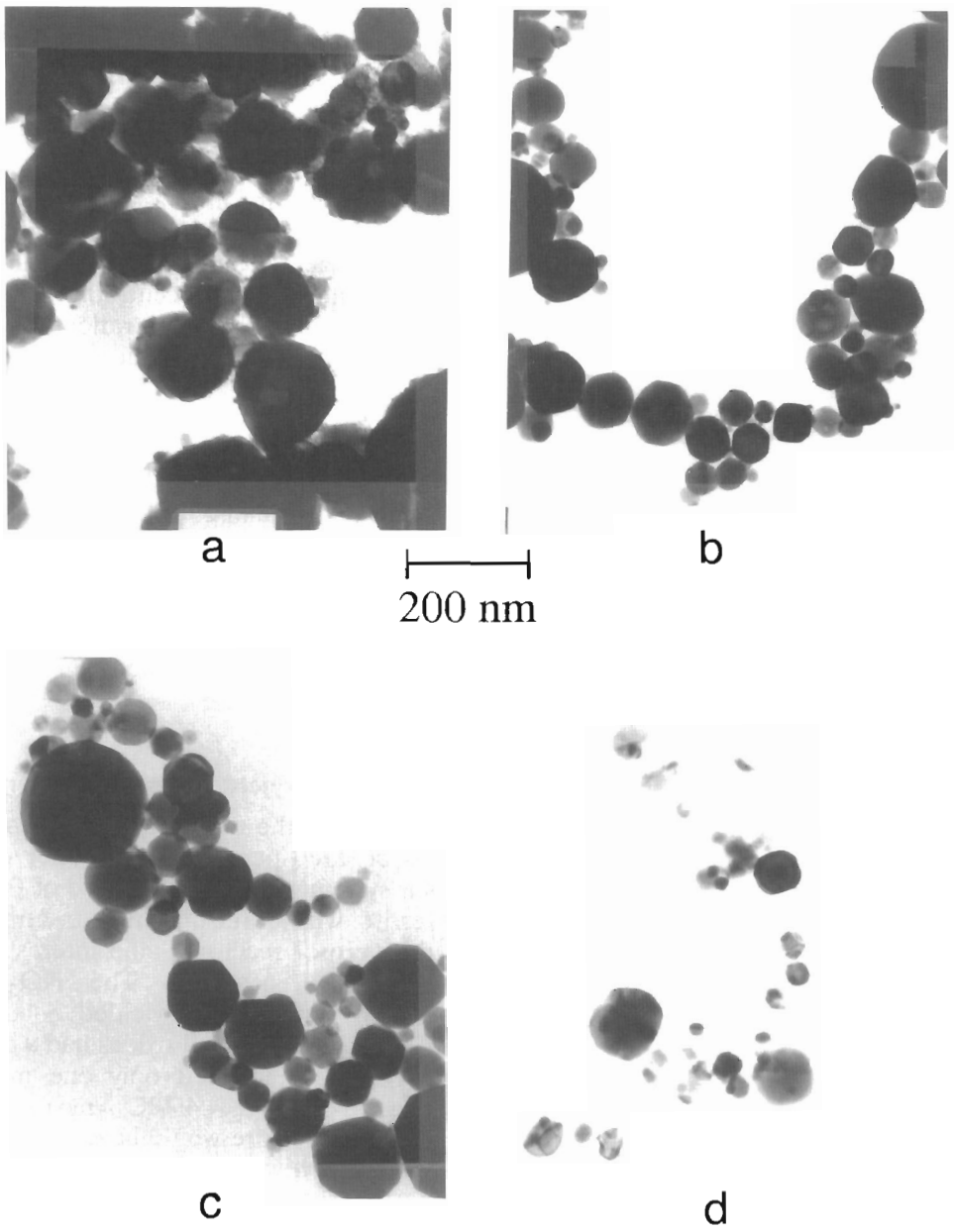

FIGURE 6. TEM micrographs of as-prepared particles for various conditions; (a) NO_3/Cl precursor, 250 + 1050°C reactor; (b) NO_3/NO_3 precursor, 900 + 1050°C reactor; (c) NO_3/NO_3 precursor, 900 + 1250 + 900°C reactor; (d) NO_3/NO_3 precursor, 1/10 normal concentration (i.e., $[Fe^{+3}] + [Mn^{+2}] = 0.00875$ M), 900 + 1050°C reactor.

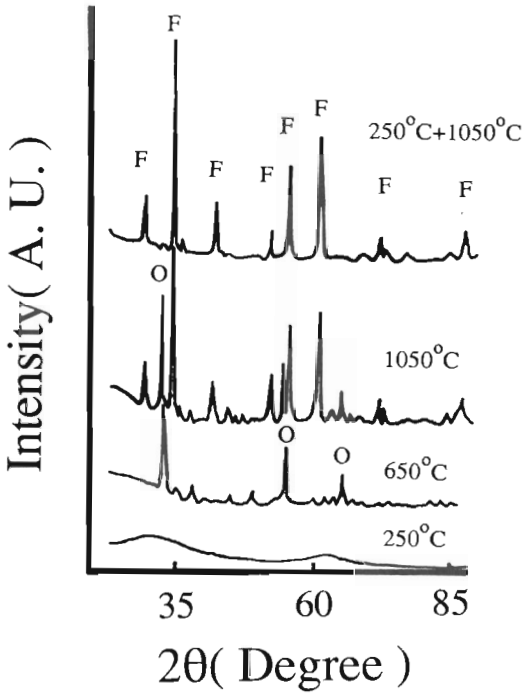

FIGURE 7. XRD spectra for a NO_3/NO_3 precursor as-prepared particles for various aerosol reactor conditions. *F* designates major $MnFe_2O_4$ lines, O designates major lines of Fe_2O_3 or Mn_2O_3, which have similar spectra.

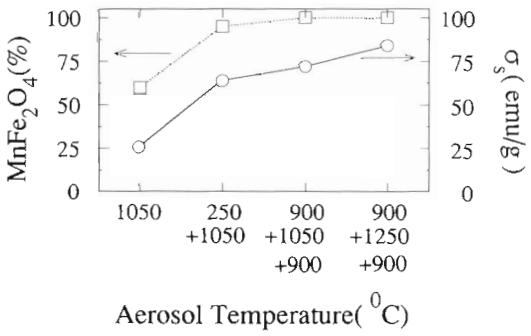

FIGURE 8. Percentage fraction of $MnFe_2O_4$ and saturation magnetization σ_s at 300K as a function of aerosol reactor conditions for as-prepared, NO_3/NO_3 precursor particles.

NO_3/NO_3 precursor system having passed through a two-stage, 900 + 1050°C reactor and three-stage 900 + 1250 + 900°C reactor, respectively. The particles are dense and polygonal in shape, indicating the crystal habit of the material. The mean particle size is $d \sim 80$ nm, significantly less than for the as-prepared 650°C aerosol reactor particles, no doubt a result of the densification. No agglomeration or necking has occurred.

The precursor concentration was cut by half and a tenth to produce smaller particles. Figure 6d shows the particles produced with total metal concentration one-tenth the standard system ($[Fe^{+3}] + [Mn^{+2}] = 0.00875$ M). The morphology is again that of dense, polygonal, unagglomerated particles.

To conclude we see that with sufficient reactor heating, dense, single-phase, unagglomerated particles of $MnFe_2O_4$ can be created in a one-step aerosol spray pyrolysis procedure.

Aerosol Products: Magnetic Properties

In general, the magnetic properties of the as-prepared particles from either precursor system were close to those of the bulk ferrite with sufficient heat treatment in the aerosol reactor. Some interesting effects also occurred. The NO_3/NO_3, 1050°C system which yielded $\sim 60\%$ ferrite plus single metal oxides had a σ vs. T curve that indicated only one magnetic phase with a $T_c = 490$K. Any mixture of oxide and ferrite would have a complex σ vs. T graph with T_c values of the individual phases; yet this is not observed. We cannot now explain this result.

The mean particle size was varied by changing the precursor concentration. Figures 9 and 10 show saturation magnetization σ_s and coercivity H_c, respectively, as a function of mean particle size observed with TEM. In other work we have created $MnFe_2O_4$ particles by aqueous

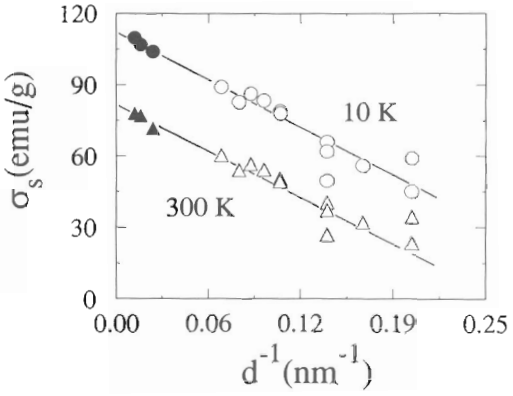

FIGURE 9. Saturation magnetization σ_s versus inverse mean particle diameter at two temperatures for as-prepared, NO_3/NO_3 precursor, 900 + 1050°C reactor particles (*solid symbols*). Also included are data for $MnFe_2O_4$ particles prepared by aqueous phase precipitation (*open symbols*). The lines are guides for the eye.

phase precipitation methods in the size range 5–25 nm (Tang et al., 1991a, b; Chen et al., 1993). Figure 9 contains σ_s versus inverse diameter for both the aerosol and aqueous phase prepared particles. In our aqueous phase precipitation work we had interpreted the linear behavior of σ_s vs. d^{-1} as due to the presence of a magnetically less active or inert surface layer of constant thickness (ca. several angstroms) on the particles. Figure 10 shows our aerosol particles are in accord with this behavior in the large size limit, and hence the inference is that a similar layer exists on the aerosol particles as well. Values of H_c for both systems of particles are plotted in Figure 10 and one does not see a unity of behavior between the aerosol prepared and solution prepared particles. Decreasing H_c with increasing size and temperature is typical of multidomain particles. This behavior is seen for the aerosol particles and implies the single domain size is less than ~ 40 nm for aerosol synthesized particles. The mechanism for the coercivity for these two systems may be different, possibly due to a difference in the single domain size.

Figure 11 shows the temperature dependence of the saturation magnetization plotted to test Bloch's Law (Cullity, 1972)

$$\sigma_s(T) = \sigma_s(0)(1 - BT^{3/2}). \tag{3}$$

When σ_s vs $T^{3/2}$ is plotted, the graph should be linear and the slope will yield

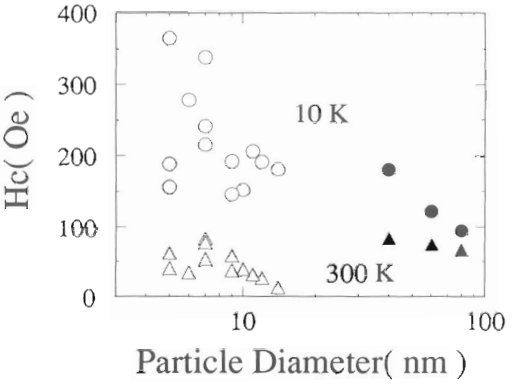

FIGURE 10. Coercivity H_c as a function of mean particle diameter at two temperatures for as-prepared, NO_3/NO_3 precursor, 900 + 1050°C reactor particles (*solid symbols*). Also included are data for $MnFe_2O_4$ particles prepared by aqueous phase precipitation (*open symbols*).

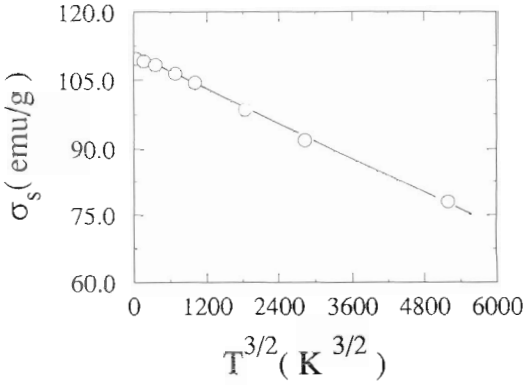

FIGURE 11. Saturation magnetization versus temperature to the 3/2 power for as-prepared, NO_3/NO_3, 900 + 1050°C reactor particles. The line is a fit to Bloch's law.

the Bloch constant B if Eq. 3 holds. The plot in Figure 11 is linear indicating Bloch's law holds. The slope yields a Bloch constant of $B = 5.6 \times 10^{-5}$ $K^{-3/2}$. This value is roughly equal to the value determined for our largest particles prepared by aqueous phase precipitation. These latter particles show B to increase with decreasing particle size, a result seen in (Gangopadhyay et al. 1992) and predicted for (Mills, 1971) other systems. Unfortunately, we do not know the bulk value of B for comparison to the aerosol particle value to determine if the size dependence is present in these particles as well.

Finally, we note for phase pure ferrite particles the Curie temperatures are all near $T_c \simeq 590$K (Table 2). This is close to the value found earlier for rapidly cooled specimens due to the A/B site distribution of the Mn ions. The aerosols are, by the nature of the production process, rapidly cooled as they leave the reactor. Hence the high T_c values, which could be annealed downward by reheating followed by slow cooling.

CONCLUSION

Aerosol spray pyrolysis can be used successfully to create in a one-step process submicrometer particles of manganese ferrite which are dense, nonagglomerated, and both chemically and magnetically single phase. The key to obtain these favorable properties is that the aerosol reactor must be at a sufficiently high temperature, in excess of 900°C for manganese ferrite.

Without sufficient heating one sees the defects commonly encountered with this technique: hollow and porous particles with incorrect chemical phase. Following Charlesworth and Marshall (1960), it is reasonable to propose the hollow structures we observed are due surface precipitation of precursors during the rapid drying phase of the droplets. We believe the porosity is due to subsequent loss of water of hydration and the anions. We argued that phase segregation was a chemical effect, chemical segregation, owing to the tendency for manganese to be oxidized from the divalent to trivalent form, especially in the presence of nitrate. The divalent form of manganese is necessary for the ferrite. Postaerosol baking above 900°C both densified the particles and caused their evolution to the pure ferrite phase, but also caused particle sintering and agglomeration.

We believe an important lesson learned is that despite the various causes of poor morphology or phase, a viable solution is simply aerosol processing at sufficiently high temperature. Such a solution has recently been suggested by others (Chadda et al., 1991; Ortega and Kodas, 1992).

The manganese ferrite particles we created had magnetic properties roughly equal to bulk manganese ferrite particles. The saturation magnetization showed some size dependence possibly due to a magnetically inactive surface layer. This effect for our aerosol particles corresponded well with a similar effect in smaller manganese ferrite particles made by aqueous phase precipitation. The coercivity increased with decreasing particle size to imply a multidomain character. Comparison to aqueous phase precipitation particles showed that differences may exist in the coercivity mechanism of these two systems. The Bloch constant was consistent with that found for aqueous phase precipitated particles. The Curie temperature was cooling rate dependent, and since the aerosol method involved quick cooling of the particles as they leave the reactor, these particles had Curie temperature ~ 30K higher than expected for slowly cooled particles.

We thank Afan Ottenheimer for assistance during the initial stages of this work. This work was supported by NSF Grant CHE9013930 and an equipment grant to obtain the SQUID magnetometer, NSF DMR9123831.

REFERENCES

Biswas, P., Lin, S. Y., and Boolchand, P. (1992). *J. Aerosol Sci.* 23:5807–5810.

Chadda, S., Ward, T. L., Carim, A., Kodas, T. T., Ott, K., Kroeger, D. (1991). *J. Aerosol Sci.* 22:601–616.

Charlesworth, D. H., and Marshall, W. R. Jr., (1960). *A.I.Ch.E.J.* 6:9–23.

Chen, J. P., Sorensen, C. M., Klabunde, K. J., and Hadjipanayis, G. C. (1993). Unpublished results.

Clearfield, A., Gadalla, A. M., Marlow, W. A., and Livingston, T. W. (1989). *J. Am. Ceram. Soc.* 72:1789–1792.

Cullity, B. D. (1972). *Introduction to Magnetic Materials.* Addison-Wesley, New York.

Gadalla, A. M., and Yu, H. F. (1990). *J. Mater. Res.* 5:2923–2927

Gangopadhyay, S., Hadjipanayis, G. C., Dale, E. B., Sorenson, C. M., Klabunde, K. J., Papaefthymiou, V., and Kostikas, A. (1992). *Phys. Rev.* B45:9778–9787.

Kodas, T. T. (1989). *Adv. Mater.* 6:180–192.

Klug, H. P., and Alexander, L. (1954). *X-Ray Diffraction Procedures for Polycrystalline and Amorphorus Materials.* Wiley, New York.

Mills, D. L. (1991). *Commun. Solid State Phys.* 4:28–30.

Ortega, J., and Kodas, T. T. (1992). *J. Aerosol Sci.* 23:5253–5256.

Ortega, J., Kodas, T. T., Chadda, S., Smith, D. M., Ciftcioglu, M., and Brennan, J. E. (1991). *Chem. Mater.* 3:746–751.

Roy, D. M., Neurgaonkar, R. R., O'Holleran, T. P., and Roy, R. (1977). *Ceram.Bull.* 56:1023–1024.

Ruthner, M. J. (1983). *Ceram. Powders.* 515–531.

Simsa, Z., and Brabers, V. A. M. (1975). *IEEE Trans. Mag.* 11:1303–1305.

Sproson, D. W., Messing, G. L., and Gardner, T. J. (1986). *Ceram. Int.* 12:3–7.

Tang, Z. X., Nafis, S., Sorensen, C. M., Hadjipanayis, G. C., and Klabunde, K. J. (1989a). *IEEE Trans. Mag.* 25:4236–4238.

Tang, Z. X., Nafis, S., Sorensen, C. M., Hadjipanayis, G. C., and Klabunde, K. J. (1989b). *J. Mag. Mag. Mater.* 80:285–289.

Tang, Z. X., Sorensen, C. M., Klabunde, K. J., and Hadjipanayis, G. C. (1991a). *J. Colloid Interface Sci.* 146:38–52

Tang, Z. X., Sorensen, C. M., Klabunde, K. J., and Hadjipanayis, G. C. (1991b). *Phys. Rev. Lett.* 67:3602–3605.

Weast, R. C. (1977). *Handbook of Chemistry and Physics.* CRC, Cleveland, OH, Vol. 57.

Xu, H. K., Sorensen, C. M., Klabunde, K. J., and Hadjipanayis, G. C. (1992). *J. Mater. Res.* 7:712–716.

Yasuoka, H., Hirai, A., Shinjo, T., Kiyama, M., Bando, Y., and Takada, T. (1967). *J. Phys. Sec. Jpn.* 22:174–180.

Zhang, S. C., Messing, G. L., and Huebner, W. (1991). *J. Aerosol Sci.* 22:585–599.

Zhang, S.-C., Messing, G. L., and Borden, M. (1990). *J. Am. Ceram. Soc.* 73:61–67

Received February 1, 1993; accepted May 21, 1993.